Lynx, n. s. (Praha), **53**: 185–205 (2022). ISSN 0024-7774 (print), 1804-6460 (online)

On the retinae of *Glis* and *Graphiurus*: photoreceptor and ganglion cell populations, an absence of shortwave-sensitive cones, and some other features (Rodentia: Gliridae)

Leo PEICHL[1], Tijana RADIC[1], Irina SOLOVEI[2], Michael WOLFRAM[3] & Martin GLÖSMANN[3]

[1] Institute of Clinical Neuroanatomy, Dr. Senckenbergische Anatomie, Goethe University, D–60590 Frankfurt am Main, Germany; Peichl@em.uni-frankfurt.de
[2] Biozentrum, Ludwig Maximilians University Munich, D–82152 Planegg-Martinsried, Germany
[3] VetCore Facility for Research, University of Veterinary Medicine Vienna, A–1210 Vienna, Austria

received on 27 August 2022

Abstract. The retina of the fat dormouse *Glis glis* was studied histologically. Opsin immunolabeling identified an unusually dense population of rod photoreceptors (ca. 600,000–780,000/mm²) and a low-density population of L cone photoreceptors containing the longwave-sensitive (LWS) cone opsin, with a shallow maximum of ca. 3,300/mm² in temporal retina and ca. 2,000–3,000/mm² in the remaining retina. Hence the cones comprise only 0.25–0.50% of the photoreceptors. There are no S cones expressing the shortwave-sensitive (SWS1) opsin that is the second cone opsin in most mammals, conveying dichromatic colour vision. We conclude that the fat dormouse is a cone monochromat. Sequencing of the tuning-relevant exon 1 of the SWS1 opsin gene revealed that the gene would have coded for a UV-sensitive visual pigment, but that it contains mutational changes making it nonfunctional. Retinal interneurons (rod bipolar cells, horizontal cells, several amacrine cell types) have rodent-typical features. NeuN-labeled presumed retinal ganglion cells have densities between ca. 4000/mm² in temporal central retina and 850–1300/mm² in peripheral retina. The peak ganglion cell density would result in an estimated visual acuity maximum of ca. 1.8 cycles/degree or ca. 33 minutes of arc. Assessment of a further Gliridae species, the African dormouse *Graphiurus* sp., also revealed a high rod density, low L cone density, and an absence of SWS1 opsin.

Key words. Rodent retina, fat dormouse, *Glis glis*, African dormouse, *Graphiurus*, rod photoreceptors, cone photoreceptors, SWS1 opsin loss, visual acuity.

INTRODUCTION

The European and African dormice are nocturnal omnivores belonging to the family Gliridae in the rodent suborder Sciuromorpha. The fat dormouse *Glis glis*, also termed edible dormouse, is found throughout most of Europe and parts of western Asia. A summary of *G. glis* biology is given by Kryštufek (2010). It has a compact body of 130–190 mm length and a long bushy tail. It is very arboreal, its preferred habitats are deciduous and mixed woodlands as well as orchards, but buildings close to woodlands are also frequently inhabited. There, the fat dormouse is a nuisance because of the damage it causes to structures and stores, and because of its nocturnal noise (Büchner et al. 2018). *Glis glis* hibernates for 7–8 months over the winter. Historically, fat dormice were hunted for their fur and meat. The African dormice (genus *Graphiurus*) live

doi: 10.37520/lynx.2022.013

throughout sub-Saharan Africa, where they inhabit forests and savannah. They are also arboreal, but frequently found on the ground.

The retinae of dormice have not been studied to date. The only reference we found is a brief statement in a German handbook article by Kolmer (1936: 326), where he writes that cone photoreceptors are certainly missing in bats and dormice. Given that bats have since been shown to possess cones (Müller et al. 2007, 2009), that statement certainly needed checking with present day methods. Hence, when the opportunity arose, we studied the retinae of the fat dormouse and a *Graphiurus* species, focusing on the photoreceptors. The mammalian retina is a 'duplex retina' possessing rod photoreceptors for low-light vision and cone photoreceptors for daylight and colour vision. Most non-primate mammals have limited, dichromatic colour vision based on the presence of two spectral cone types (reviews: Jacobs 2009, Ahnelt & Kolb 2000, Peichl 2005). The standard set are longwave-sensitive L cones containing the opsin LWS (typically green-sensitive) and shortwave-sensitive S cones containing the opsin SWS1 (blue, violet, or UV sensitive). The majority of mammals, even most diurnal species, have a dominant population of rod photoreceptors. We were interested to learn how the dormice fit into this mammalian retinal blueprint, and also included the retinal ganglion cells and some relevant interneurons in our analysis. Preliminary unpublished data by Martin Glösmann on the S opsin loss in *Glis glis* were mentioned by Ahnelt & Kolb (2000) and Ahnelt et al. (2003).

MATERIAL AND METHODS

Animals and tissue preparation

The eyes of seven adult *Glis glis* individuals (three females, two males, two of unknown sex) were available for this study. The animals lived under the roofs of an isolated farm located in a partly forested area in the German State of Hessen, and the farmer's cats sometimes brought in freshly killed adult individuals. Killings occurred in July and August, i.e. not during the hibernation phase of the animals. *Glis glis* is a protected species according to German law (Bundesartenschutzgesetz BArtSchG, Appendix 1), but it is allowed to use animals in this protection group for scientific research when found dead (Bundesnaturschutzgesetz BNatSchG, § 45/4). The farmer, who also is a hunter with experience in dissecting game, was instructed to extract and fix the *Glis glis* eyes with instruments and reagents that we had provided. We can assume that fixation began less than an hour *post mortem*. The eyes were immersion-fixed for between 2 and 4 hours in 4% paraformaldehyde (PFA) in phosphate buffer (PB, pH 7.4) at ambient temperature, and then transferred to PB containing 0.05% sodium azide (PB+NaN_3) for transport to the laboratory and further handling. The two eyes of an old *Graphiurus* sp. (most likely *G. parvus*, but perhaps *G. murinus*) individual that had died in Moscow Zoo were provided to us by our Russian colleagues Vladimir Lebedev (Zoological Museum of Moscow State University, Moscow) and Svetlana Romanenko (Institute of Molecular and Cellular Biology SB RAS, Novosibirsk). The conservation status of the species is "least concern", so no permits were required for use of the material. Shortly post mortem, the eyes were fixed for 1 day in 4% PFA, washed in phosphate buffered saline (PBS), infiltrated with sucrose, and frozen in 30% sucrose in PBS at –20 °C for transport and storage.

In the laboratory, the *G. glis* external eye dimensions were determined with calipers, the eyes were cut open behind the cornea, and the posterior eyecup with attached retina was either processed immediately or stored for later processing of the retina. Some eyecups were stored in PB with 0.05% sodium azide at 4 °C. Some eyecups were cryoprotected by successive immersion in 10%, 20% and 30% (w/v) sucrose in PB with 0.05% sodium azide and stored frozen at –20 °C. The *Graphiurus* eyes were also stored frozen. Here, no measurement of the eye dimensions was done.

For staining, the retina was carefully dissected from the eyecup. When remains of retinal pigment epithelium (RPE) were still attached to retinae intended for photoreceptor staining, the RPE was bleached by

immersion in a bleaching solution (Hemmi & Grünert 1999). After bleaching, the retina was thoroughly washed in PB. For frozen vertical sections of the retina (i.e., sections perpendicular to the retinal layers), pieces of retina were transferred from 30% sucrose to tissue freezing medium (Leica Biosystems, Wetzlar, Germany), flattened, frozen, sectioned at 14–16 µm thickness with a cryostat (Leica CM 3050 S, Wetzlar, Germany), and collected on Superfrost Plus slides (Menzel Gläser, Braunschweig, Germany).

Immunohistochemistry

Immunohistochemical analyses were performed on sectioned and flatmounted retinal tissue with the primary antibodies listed below. Antibodies were diluted in PBS, pH 7.4, containing 0.5% Triton X-100 and 0.02% sodium azide with 3% normal donkey serum. Immunolabeling was performed using the indirect fluorescence method. Incubation with the primary antibodies was overnight for cryostat sections, and for 2–3 days for unsectioned retinal pieces and whole retinae, followed by a 1 h incubation (sections) or a 1.5–2 h incubation (free-floating pieces) in the secondary antibody solutions, which were conjugated to Alexa Fluor 488, Alexa Fluor 647 (dilution 1:500; Invitrogen), Cy3, or Cy5 (dilution 1:250; Dianova). In double- and triple-labeling experiments, tissue was incubated in a mixture of primary antibodies, followed by a mixture of secondary antibodies.

Primary antibodies and cell markers: The fluorescent Nissl stain NeuroTrace 530/615 (dilution 1:100; N21482, Invitrogen) was used to label all neurons, and a rabbit monoclonal antibody against NeuN (dilution 1:100; ab177487, Abcam) to label presumed retinal ganglion cells. Rod opsin was detected with the mouse monoclonal antibody rho4D2 (dilution 1:1,000), kindly provided by R. S. Molday (Hicks & Molday 1986). The LWS cone opsin was detected with the rabbit antiserum JH 492 (dilution 1:2,000), the SWS1 cone opsin with the rabbit antiserum JH 455 (dilution 1:5,000) or the goat antiserum sc-14363 (dilution 1:500; Santa Cruz Biotechnology, Heidelberg, Germany). The antisera JH 492 and JH 455 were kindly provided by J. Nathans (Wang et al. 1992). Alexa-conjugated peanut agglutinin (PNA647, dilution 1:100; L-32460, Molecular Probes) was used as a general cone marker. Various interneuron types were labeled by a rabbit antiserum against protein kinase C α (PKCα, dilution 1:5000; P4334, Sigma), a goat antiserum against choline acetyltransferase (ChAT, dilution 1:200; AB144P, EMD Millipore), a rabbit antiserum against calbindin CaBP-28k (dilution 1:2,000; CB38, Swant), a rabbit antiserum against parvalbumin (PV, dilution 1:2000; PV4064, Swant), and a mouse monoclonal antibody against the neurofilament heavy chain NF200 (dilution 1:500; clone N52, N0142, Sigma). Omission of the primary antibodies from the incubation solution resulted in no staining. Sections were counterstained with DAPI to show the retinal layering. The nuclear architecture in rods and other retinal neurons was assessed by immunostaining of the euchromatin-specific histone modification marker H3K4me3 (dilution 1:200, ab8580, Abcam) in combination with DNA counterstaining by DAPI serving as a heterochromatin marker.

In the two JH 492-labeled retinae used for the topographical analysis of L cone densities, and in one retina labeled for calbindin, incubation with the primary antiserum was followed by an overnight incubation in goat anti-rabbit IgG, an overnight incubation in rabbit peroxidase-antiperoxidase (PAP) complex, and visualization with 3,3'-diaminobenzidine (DAB) and H_2O_2. All tissue was coverslipped with an aqueous mounting medium (AquaPoly/Mount, Polysciences, Warrington, PA, USA).

Image acquisition and quantifications

Immunofluorescence-labeled vertical sections and retinal pieces were analyzed with a laser scanning microscope (LSM) Olympus FluoView 1000 using the FV10 ASW 3.1 software (Olympus) and 20×/0.75 UPlanSApo and 40×/0.95 UPlanSApo objectives, using the zoom function when necessary. LSM images and z-stack projections were examined with ImageJ, cells were counted using the Cell Counter plugin of ImageJ. Images for illustration were adjusted for brightness and contrast using Adobe Photoshop. Unless stated otherwise, projections of confocal stacks are shown. For convenience, fluorescent images are shown in pseudocolours. PAP/DAB-reacted tissue was analyzed with a Zeiss Axioskop 2 microscope by differential interference contrast, micrographs were taken with a CCD camera. For analysis of the euchromatin

and heterochromatin distribution, single focus images were collected from vertical sections using a Leica TCS SP5 confocal microscope equipped with a Plan Apo ×63/1.4NA oil immersion objective.

To analyse the L cone distribution in a PAP/DAB-reacted, flatmounted whole retina, about 100 sampling fields spaced at regular intervals across the retina were counted manually at a Zeiss Standard brightfield microscope equipped with a drawing tube. Sampling field sizes were 250×250 µm. Photoreceptor densities were not corrected for potential shrinkage.

SWS1 opsin sequencing

To assess the spectral tuning of the SWS1 opsin (UV-sensitive vs. violet/blue-sensitive), we sequenced segments of the SWS1 opsin gene relevant for determining the spectral sensitivity of the visual pigment. Genomic DNA was extracted from ethanol-preserved muscle tissue. Primers 5'-GAGGTTTGGGTGAG-GGCTTT-3' and 5'-AGCCCAGAAACAAGGAGAGG-3' were used for PCR amplification of exon 1 of the SWS1 opsin gene. Reactions were conducted in 25 µL volumes on a Mastercycler Nexus Gradient (Eppendorf, Hamburg, Germany) with initial denaturation at 95 °C for 12 minutes, denaturation at 95 °C for 30 seconds, annealing at 58 °C for 30 seconds, extension at 72 °C for 60 seconds for 35 cycles, followed by a final extension at 72 °C for 7 minutes. A single 922 bp product was amplified, purified, and sequenced on both strands.

Visual acuity estimate

An estimate of visual acuity can be obtained from the maximum ganglion cell density and the axial length (AL) of the eye. According to Pettigrew et al. (1988), the posterior nodal distance (PND) of the eye's optical system is PND = 0.52×AL for nocturnal mammals, and the retinal magnification factor (RMF) that gives the image size per degree of visual angle on the retina is:

$$\text{RMF [mm/deg]} = 2\pi \times (\text{PND [mm]}) / (360 \text{ [deg]})$$

The visual acuity in cycles per millimetre on the retina is:

$$\text{Visual acuity [cyc/mm]} = (\sqrt{\text{maximal ganglion cell density [mm}^{-2}\text{]}}) / 2 \text{ [cyc}^{-1}\text{]}$$

and the visual acuity in cycles per degree of visual angle is:

$$\text{Visual acuity [cyc/deg]} = \text{RMF [mm/deg]} \times \text{Visual acuity [cyc/mm]}$$

RESULTS

General eye and retina features

Ten eyes of five *Glis glis* individuals were measured. Their mean axial length was 6.26±0.23 mm SD (range 6.0–6.7 mm), their mean equatorial diameter was 6.54±0.26 mm SD (range 6.2–6.8 mm), their mean corneal diameter was 5.64±0.22 mm SD (range 5.4–6.0 mm), their mean lens diameter was 4.62±0.19 mm SD (range 4.3–4.9 mm), and their mean lens thickness was 3.82±0.21 mm SD (range 3.5–4.2 mm). These size data are biologically relevant: (i) The axial length determines the retinal magnification factor, i.e., how large the image size is on the retina, how many micrometers on the retina correspond to 1° of visual angle. This is taken up below where visual acuity is considered. (ii) The light collecting ability of a vertebrate eye depends on corneal size (a proxy for maximal pupil size) and focal length of the lens; a larger cornea and thicker lens (i.e., of shorter focal length) provide more light to the retina (see, e.g., Kirk 2006, Land & Nilsson 2002, Schmitz & Motani 2010).

In *Glis glis*, the relative corneal size (corneal diameter expressed as a percentage of the eyes' equatorial diameter) was 86%. Such a relatively large corneal diameter indicates that the eyes can efficiently capture light and is typical for nocturnal mammals. Correspondingly, the lens diameter also was relatively large, having 71% of the eye's equatorial diameter and 82% of the corneal diameter. The lens thickness expressed as a percentage of the eye's axial length was 61%, which also is typical for nocturnal mammals, as a thicker lens with a shorter focal length produces a smaller but brighter image. We have no comparable eye dimension data for the African dormouse *Graphiurus*.

The fundus of the *G. glis* eyes did not have a reflecting tapetum lucidum behind the retina. The retinae were vascularized by several major blood vessels that exited from the optic nerve head located in the centre of the retina and ran radially towards the retinal periphery, branching repeatedly. This pattern is typical for many small-eyed rodents.

The *G. glis* retina was about 170–190 µm thick across most of the retina and decreased in thickness to about 70–90 µm towards the far periphery. The outer nuclear layer (ONL) was the thickest of the retinal layers, having 12–13 tiers of photoreceptor somata in central retina (Figs. 1, 2) and 5–7 tiers in far peripheral retina. Labeling with the neuron marker NeuroTrace showed the retinal layering and revealed an inner nuclear layer (INL) having about 3 tiers of somata that are those of bipolar cells, horizontal cells, amacrine cells, and Müller glia cells; the ganglion cell layer (GCL) had only one tier of somata (Fig. 1). The *Graphiurus* sp. retina was similarly structured, ca. 160–170 µm thick, showing a thick ONL with 10–11 tiers of photoreceptor somata, an INL with about 4 soma tiers, and a single-tiered GCL (Figs. 1, 2).

Rod photoreceptors

The rod dominance of the *Glis glis* and *Graphiurus* retinae was obvious in vertical sections where the rods were labeled by a rod opsin-specific antibody (Fig. 2). As it is common in mammals, the rod opsin antibody rho4D2 intensely labeled the rod outer segments and less intensely the rod somata. The latter filled the ONL, and the rod outer segments formed a densely packed layer at the outer retinal surface Fig. 2A, B).

Glis glis rod densities were determined directly in a flatmounted retinal piece, where the rod inner segments had maintained their vertical orientation during mounting and could be counted in end-on view (Fig. 2E). In mid-peripheral retina, at locations suitable for analysis, rod densities were between 600,000 and 780,000/mm². Further estimates of rod density were obtained from the density of ONL somata in vertical retinal sections (Figs. 1, 2). They were similar to the above values for central and mid-peripheral retina, and decreased to ca. 400,000 rods/mm² in far peripheral retina where the ONL was reduced to 5–7 tiers of somata. The ONL soma counts also included the cone somata, but the cone density is so low (see below) that the counts can be equaled to rod counts. For *Graphiurus*, a limited rod density estimate from DAPI-labeled vertical sections yielded about 395,000–490,000 rods/mm², with a decrease to ca. 280,000/mm² in far peripheral retina. Hence, if confirmed by further studies, the *Graphiurus* rod density is markedly lower than that of *G. glis*.

In practically all animal cells the euchromatin is located in the centre of the nucleus and the heterochromatin in the nuclear periphery. In contrast, the rod nuclei of nocturnal mammals have a unique inverted chromatin architecture with heterochromatin aggregated in the nuclear centre and euchromatin arranged at the nuclear periphery (Solovei et al. 2009). This was also the case in the nocturnal *Glis glis* and *Graphiurus* (Fig. 2C, D). Often, the rod nuclear central heterochromatin cluster had a fold with some embedded euchromatin (Fig. 2C2). All other retinal

cells, including the cones, had the conventional nuclear architecture (cone nuclei are marked by arrowheads in Figs. 2C1 and C3, a ganglion cell is shown in Fig. 2D3). The functional implications of the inverted rod nuclear architecture are addressed in the Discussion.

Cone photoreceptors

Glis glis and *Graphiurus* cones were assessed by the general cone marker peanut agglutinin (PNA) and by antisera against the longwave-sensitive (LWS) and the shortwave-sensitive (SWS1) cone opsins. The cone population is analysed most conveniently in flat preparations.

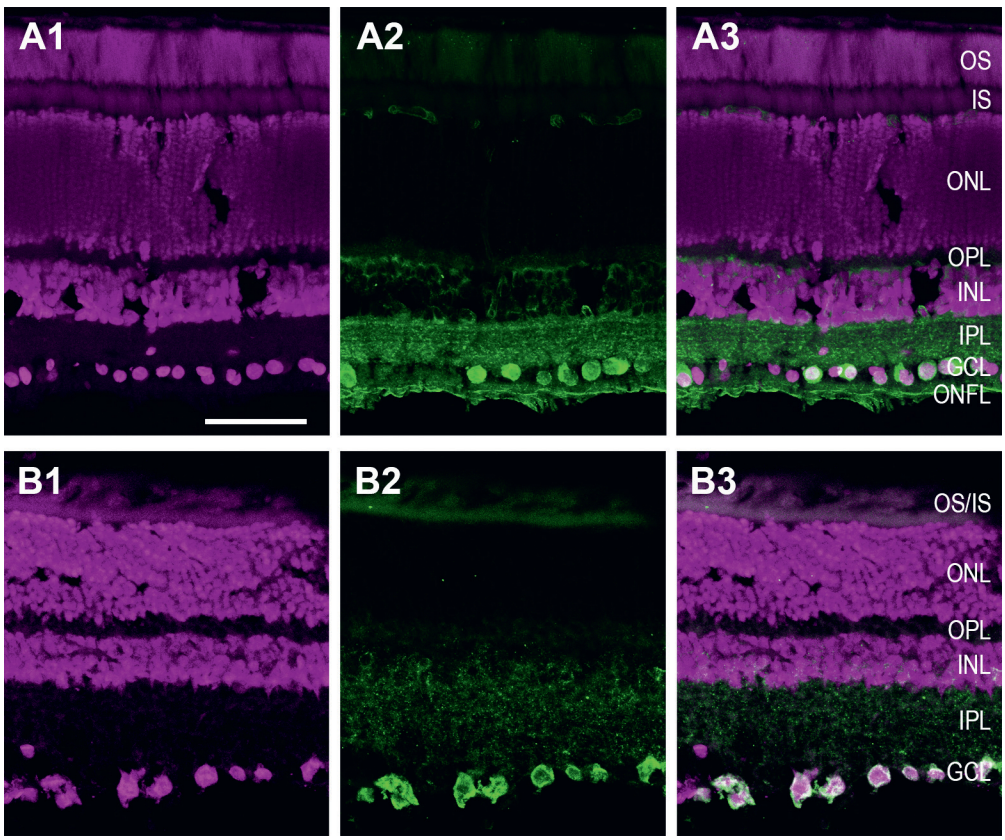

Fig. 1. Retinal morphology of *Glis glis* (A) and *Graphiurus* sp. (B) in vertical sections. (A1, B1) NeuroTrace labeling (magenta), (A2, B2) NeuN labeling (green), (A3, B3) merge. NeuroTrace labels the neurons in all retinal soma layers, NeuN is only present in presumed retinal ganglion cells in the ganglion cell layer (GCL). NeuroTrace-positive and NeuN-negative somata in the GCL are presumed displaced amacrine cells. For details see text and Fig. 6. OS, photoreceptor outer segments; IS, photoreceptor inner segments; ONL, outer nuclear layer; OPL, outer plexiform layer; INL, inner nuclear layer; IPL, inner plexiform layer; ONFL, optic nerve fibre layer. Scale bar in (A1) is 50 µm and applies to all images.

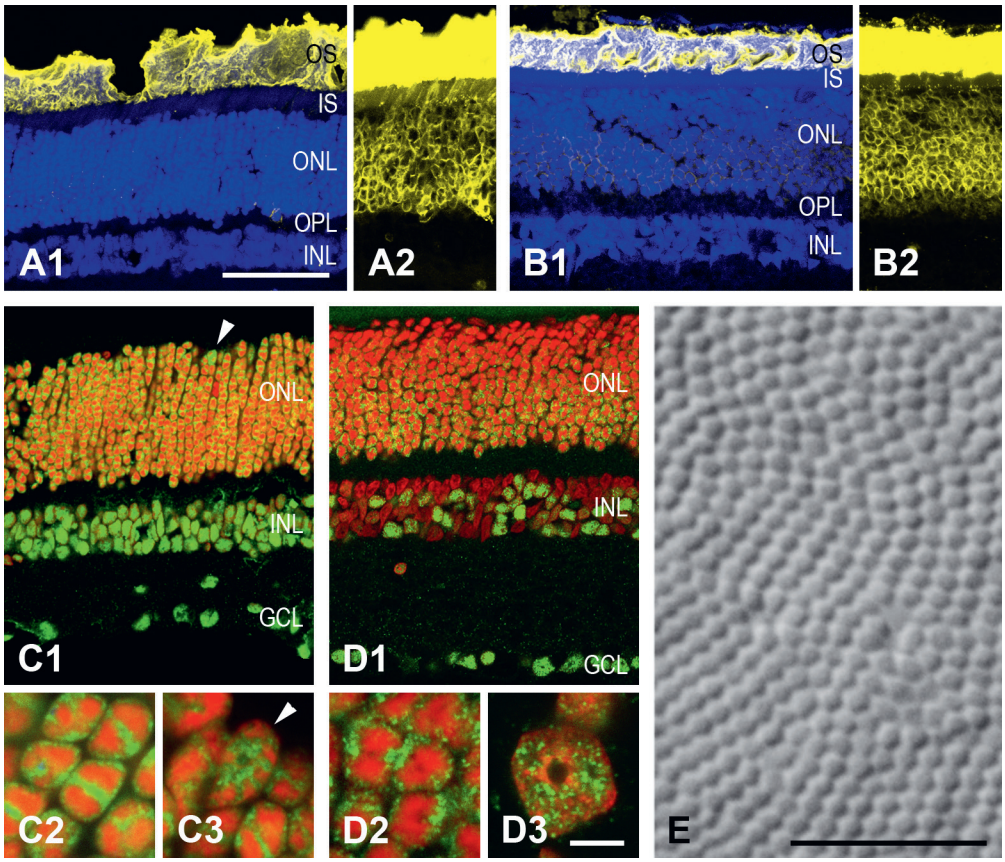

Fig. 2. Gliridae rod photoreceptors. (A1) Retinal vertical sections of *Glis glis* show a dense population of outer segments (OS) intensely immunolabeled for rod opsin (yellow); single OS cannot be recognized in this dense label; DAPI labeling of nuclear layers (blue). Overexposure shows less intense labeling also in the rod somata in the ONL (A2, showing part of A1, without DAPI). (B1, B2) The same labeling is seen in *Graphiurus* sections. (C, D) The rod nuclei in the ONL show an inverted architecture with heterochromatin (DAPI label, red) clumped in the nuclear centre, and euchromatin (anti-H3K4me3 label, green) at the nuclear periphery in *G. glis* (C1) and *Graphiurus* (D1) that is clearly seen in these overviews; enlargements of rod nuclei shown in (C2, D2). Other neurons have conventional nuclei with euchromatin located centrally, as illustrated by cone nuclei (arrowheads in C1, C3) and a ganglion cell nucleus (D3). (E) Differential interference contrast image of the rod inner segments (IS) in a flatmounted *G. glis* retina, showing the dense rod population. The cones present in this field cannot be discriminated, but they comprise <1% of the photoreceptors. (C–E) are single focus images. Retinal layers labeled as in Fig. 1. Scale bar in (A1) is 50 µm and applies to (A–D1); scale bar in (D3) is 5 µm and applies to (C2, C3, D2, D3); scale bar in (E) is 10 µm.

Flatmounted retinal pieces of both species revealed a low-density population of cones having outer segments labeled by the LWS opsin antiserum and inner segments labeled by PNA (Fig. 3A1,

Table 1. Tuning-relevant amino acids of the mammalian S cone opsin

order	species	λ_{max} (nm)	52	86	93	114	118
Rodentia	*Glis glis**		Thr	Phe	Thr	Ala	Ser
	Mus musculus	359[1]	Thr	Phe	Thr	Ala	Ser
	Rattus norvegicus	359[2]	Thr	Phe	Thr	Ala	Ser
	Cavia porcellus	400[3]	Thr	Val	Ala	Gly	Ser
	Ictidomys tridecemlineatus	437[4]	Thr	Tyr	Val	Ala	Ser
Primates	*Homo sapiens*	424[5]	Phe	Leu	Pro	Gly	Thr
Artiodactyla	*Bos taurus*	435[6]	Thr	Tyr	Ile	Ala	Cys

Tuning-relevant amino acids of the mammalian SWS1 opsins in selected species with blue or UV sensitivity. Amino acid numbers according to bovine rod opsin nomenclature (46 bovine rho = 41 mouse SWS1 cone opsin). *Mus musculus* and *Rattus norvegicus* are species with known UV tuning (maximum sensitivities given in the third column).
GenBank sequence accession numbers: *Glis glis* OP612311, *Mus musculus* NM007538.3, *Rattus norvegicus* NM031015.2, *Cavia porcellus* NM001172758.1, *Ictidomys tridecemlineatus* XM021722407.2, *Homo sapiens* NM001385125.1, *Bos taurus* NM174567.1.
Data sources: *present study, [1]Jacobs et al. (1991), [2]Jacobs et al. (2001), [3]Parry & Bowmaker (2002), [4]Jacobs et al. (1985), [5]Oprian et al. (1991), [6]Cowing et al. (2002).

C). There was no labeling of SWS1 opsin with the two used antisera sc14363 directed against an N-terminus epitope (*Glis glis*: Fig. 3A2; *Graphiurus* not illustrated) and JH455 directed against a C-terminus epitope (not illustrated). This is strong evidence that no functional SWS1 opsin is expressed, which was confirmed by partial SWS1 opsin gene sequencing (see below).

The large majority of PNA-labeled cones had an LWS opsin-containing outer segment, i.e., they are L cones. In both species, the L cone spacing was rather irregular. In *G. glis*, a small and locally varying fraction (between 2% and 10%) of the PNA-labeled cones showed neither LWS nor SWS1 labeling (arrowheads in Fig. 3A1). These may be cones with a degenerated outer segment, or cones where the outer segment had been accidentally torn off during isolation

→

Fig. 3. Gliridae cone photoreceptors. (A1, A2) Triple labeling of flat-mounted *Glis glis* retina with PNA (magenta, labeling the inner segments of all cones), LWS opsin antiserum JH492 (green, labeling the outer segments of L cones) and SWS1 opsin antiserum sc14363 (white). (A1) PNA and LWS label, (A2) SWS1 label in the same field, there is no white SWS1 label present. There are some PNA-positive cones without LWS label (three marked by arrowheads in A1), but they do not show SWS1 label. Note that PNA additionally labels a blood capillary plexus located at the border between the ONL and the cone inner segments (see text). (A1, A2) are collapsed image stacks of 6 images covering the focal levels from the cone OS to the outer ONL border. (B) Same triple labeling of flat-mounted *Graphiurus* retina. Shown is the PNA label (magenta) and LWS opsin label (green); the absent SWS1 label is not shown. Here no capillaries are labeled by PNA. Collapsed image stack of 9 images covering the focal levels from the cone OS to the outer ONL border. (C) Field from a whole flat-mounted *G. glis* retina labeled for LWS opsin (visualized with the PAP/DAB reaction); single focus image. (D) Map of the L cone topography in the retina illustrated in (C). It is a left retina seen from the photoreceptor side. The cone density peak of 3,300/mm² is marked by +; sampling fields were spaced more closely near this peak. The continuous line is the outline of the retina, the central open circle in the map marks the optic nerve head. D, dorsal; V, ventral; T, temporal; N, nasal. Scale bar in (A2) is 50 µm for (A, B); scale bar in (C) is 100 µm.

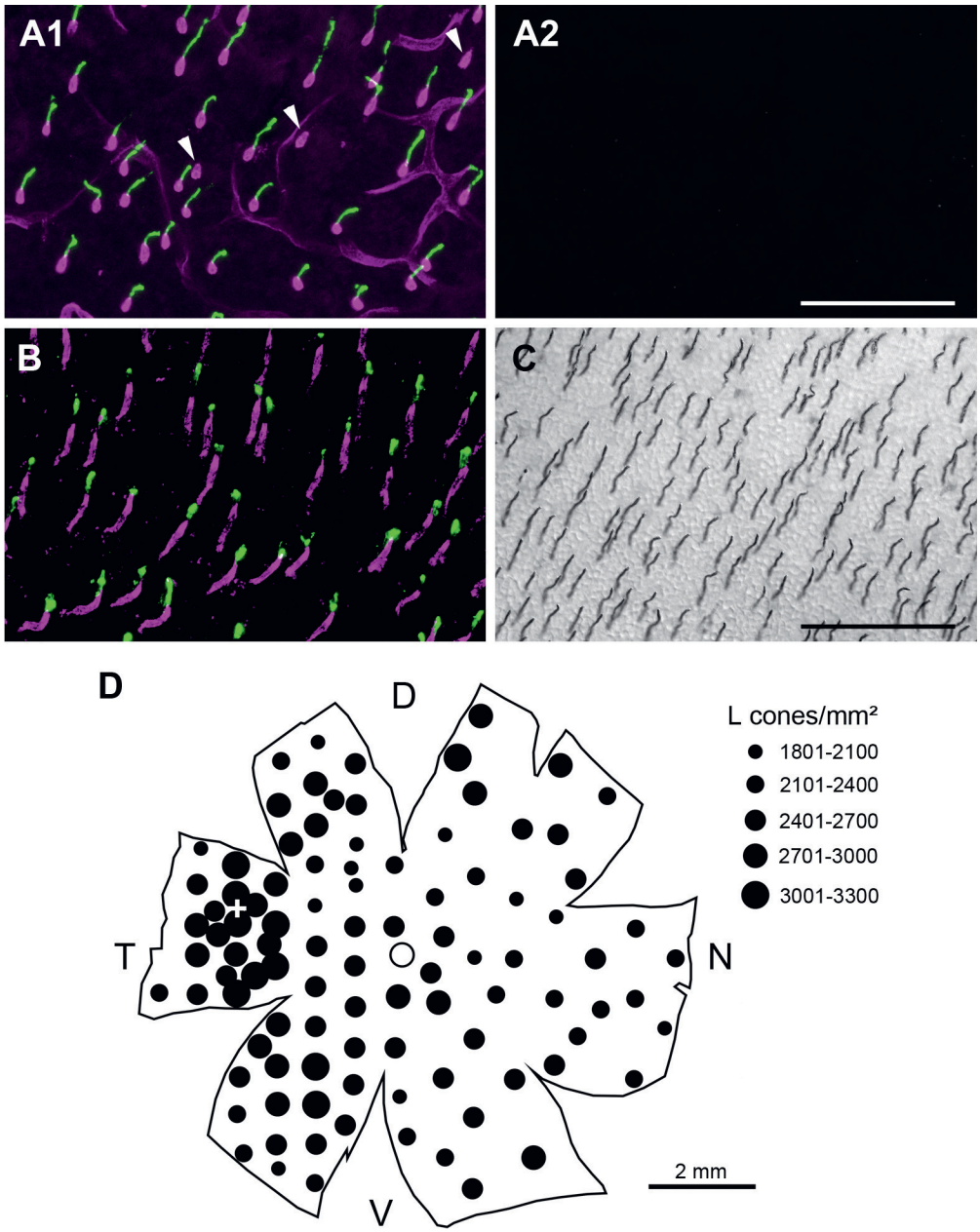
A1
A2
B
C
D
D
T
N
V
L cones/mm²
1801-2100
2101-2400
2401-2700
2701-3000
3001-3300
2 mm

of the retina. In *Graphiurus*, such PNA-positive cones without opsin labeling were very rare. A detailed analysis of *Glis glis* L cone topography was carried out in one flatmounted retina labeled by the LWS antiserum and visualized with the PAP/DAB reaction (Fig. 3C, D). The densities were confirmed at representative locations in a further LWS-labeled wholemount and in flatmounted pieces of additional retinae. There was a shallow L cone density peak of ca. 3,300/mm² in temporal retina at about 3–3.5 mm distance from the optic disc. Across the remaining retina, the densities were at about 2,000–3,000/mm², with a few locations where the density dropped to about 1,800/mm². There was no continuous decrease in cone density from the peak density location to the periphery, rather, the densities changed randomly between locations (Fig. 3D). With the *G. glis* rod densities given above, the cones constitute about 0.25–0.5% of the photoreceptors across most of the retina. In far peripheral retina, where the rod density dropped to ca. 400,000/mm² whereas the cone density did not show a similar decrease, the cone fraction may increase to 0.5–0.7%.

In selected midperipheral regions of the *Graphiurus* retina, we found L cone densities in the range of 2,200–3,200/mm², i.e., very similar to those in *Glis glis*. As we did not know the orientation of the *Graphiurus* eyes, we could not assess a cone density peak. With the rod density estimates given above, the *Graphiurus* cones would constitute 0.45–0.8% of the photoreceptors.

Glis glis SWS1 opsin sequence

The shortwave-sensitive (SWS1) cone pigment is tuned to blue/violet wavelengths in the majority of mammals. However, a number of species, among them mouse and rat, have retained the pre-mammalian ancestral tuning to UV, i.e., to wavelengths shorter than 400 nm (reviews: Hunt et al. 2007, Hunt & Peichl 2014). Hence, we were interested to learn what spectral tuning the *Glis glis* SWS1 pigment would have if it were expressed. Sequencing of exon 1 of the SWS1 opsin gene (GenBank Accession Number: OP612311) revealed two small base pair (bp) deletions, a single bp insertion, and a 233 bp insertion mutation (Fig. 4), which together would prevent the expression of a full SWS1 opsin. We aligned the fat dormouse exon 1 sequence with that of the common house mouse (GenBank Accession Number: NM_007538.3) to reconstruct codon identities at the tuning-relevant amino acid sites of the hypothetical dormouse SWS1 opsin. *Glis glis* had Thr62, Phe86, Thr93, Ala114, and Ser118 (Table 1, Fig. 4), which together have been shown to suffice to UV-shift the maximum absorption of a SWS1 pigment. Hence, a *G. glis* SWS1 pigment would absorb maximally in the UV if expressed (see Discussion).

Unusual retinal vasculature in *Glis glis*

Interestingly, in *Glis glis* the PNA label additionally revealed a blood capillary plexus at the border between the ONL and the outer limiting membrane (OLM), close to the cone inner segments (Fig. 3A1). This is surprising because in mammals the retinal vascular system typically is confined to the inner retina, with the outermost capillary plexus located in the OPL. It is generally assumed that blood-filled capillaries located close to the photoreceptor outer segments would be a stronger optical obstacle obstructing the light path (Damsgaard & Country 2022). The oxygen and nutrient supply of the outer retina, i.e., of the photoreceptors, are provided by diffusion from the choroidal vascular system that lies beyond the light path. Details of the unique capillary plexus at the ONL/OLM border will be part of a separate comparative study (Peichl et al., in prep.). No capillaries were present at the ONL/OLM border in the retina of *Graphiurus* (Fig. 3B).

Retinal interneurons

The retinal interneurons comprise bipolar cells, horizontal cells, and amacrine cells. Bipolar cells transmit information from photoreceptors to ganglion cells, horizontal cells modulate this information transfer in the OPL, and amacrine cells in the IPL. The IPL of the mammalian retina is functionally and anatomically divided into an ON and an OFF sublayer. The ON sublayer, occupying the inner part of the IPL, contains the processes and synapses of neurons activated by an onset of light or by stimuli brighter than the background. The OFF sublayer, occupying the outer part of the IPL, contains the processes and synapses of neurons activated by a light offset or by stimuli darker than the background (reviews: Wässle & Boycott 1991, Wässle 2004, Euler et al. 2014). Conventionally, the IPL is divided into five equal sublaminae S1 to S5 to facilitate the description of the stratification patterns of neuronal processes (see Fig. 5A4).

In the *Glis glis* retina, we assessed some of the interneuron types using immunolabeling. The cholinergic amacrine cells are a useful marker population for the ON/OFF subdivision of the IPL and label reliably with antibodies to choline acetyl transferase (ChAT). In mammals, they come in two mirror-symmetric populations, one with the somata in the INL and the processes in the OFF sublayer, the other with the somata in the GCL (so-called displaced amacrines) and the processes in the ON sublayer of the IPL (review: Vaney et al. 2012). The ON/OFF boundary lies between these two ChAT bands. The position of the bands in the IPL and hence the

Fig. 4. *Glis glis* nucleotide sequence of exon 1 of the SWS1 opsin. Alignment of nucleotide sequences of the coding region of *G. glis* Opn1sw (= SWS1) exon 1 with that of mouse (*M. musculus*, GenBank Accession Number NM007538.3). Identical nucleotides indicated by dots. Gaps indicated by dashes inserted to optimize the alignment. Tuning-relevant sites shaded in colour, mutations present in the dormouse sequence shaded in grey. *Glis glis* shows 4 mutational defects in exon 1: a 2-bp frameshift deletion (alignment position: 23–24), a 1-bp deletion (alignment: 109), a 233-bp frameshift insertion (alignment: 131/132), and a 1-bp insertion (alignment: 231).

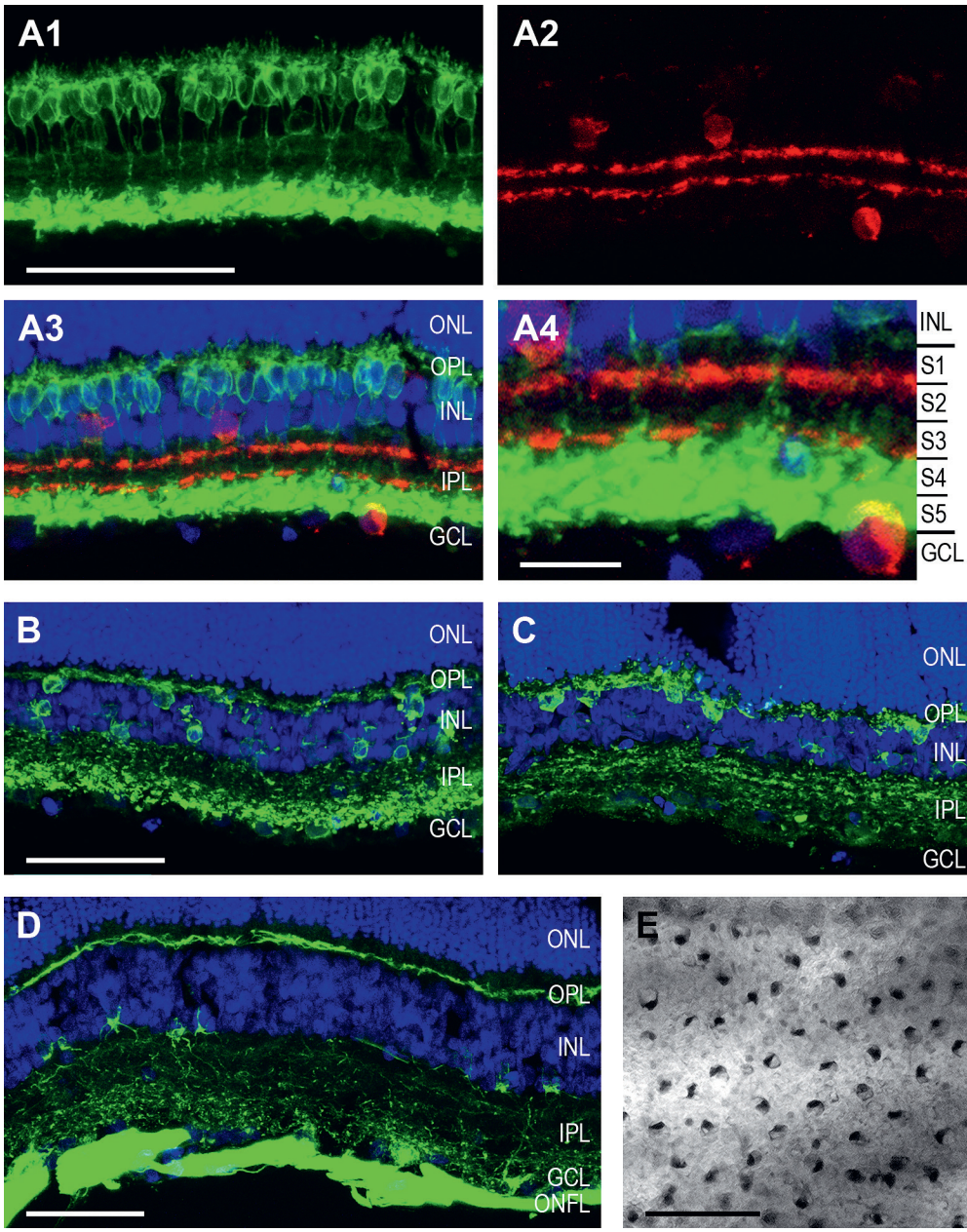
A1
A2
A3
ONL
OPL
INL
IPL
GCL
A4
INL
S1
S2
S3
S4
S5
GCL
B
ONL
OPL
INL
IPL
GCL
C
ONL
OPL
INL
IPL
GCL
D
ONL
OPL
INL
IPL
GCL
ONFL
E

Fig. 5. *Glis glis* retinal interneurons in vertical sections. (A) Section PKCα-labeled for rod bipolar cells (A1) and ChAT-labeled for cholinergic amacrine cells (A2); (A3) merge with added DAPI label (blue). (A4) enlarged part of (A3) showing the conventional division of the IPL into five equal sublaminae S1 to S5. The ChAT-labeled dendritic bands are located at the S1/S2 border and in S3, locating the functional ON/OFF boundary of the IPL approximately to S2/S3 (see text). The axon terminals of the rod bipolar cells form a broad band at the inner end of the IPL, occupying S4 and S5. This indicates their functional ON characteristic. (B) Parvalbumin labeling with DAPI counterstain. The label shows horizontal cell somata at the outer INL border and their processes in the OPL, as well as amacrine cell somata in the inner INL and their processes in the IPL, with the most intense label in the inner half of the IPL (ON layer). (C) Calbindin labeling with DAPI counterstain. The label shows horizontal cell somata and their processes in the outer INL and OPL, respectively, as well as some amacrine cell somata in the inner INL. The IPL label may represent processes of amacrine as well as ganglion cells, showing several more intensely labeled strata. (D) Labeling for the neurofilament heavy chain NF200 with DAPI counterstain. Bundles of ganglion cell axons are intensely labeled at the inner surface of the retina (ONFL). Also labeled are some ganglion cell somata in the GCL, some amacrine cell somata at the inner border of the INL with sparsely branched processes descending into the IPL, and horizontal cell processes in the OPL, but no horizontal cell somata. This is an oblique section, hence the retinal layers appear artificially thicker. The image has been overexposed to show the amacrine cells, hence the more intense label in the ONFL and OPL is saturated. (E) Flat view of the calbindin labeled horizontal cell mosaic in a PAP/DAB reacted retina. The soma spacing is rather regular (see text). Layer labels as in Fig. 1. Scale bar in (A1) is 50 µm for (A1–A3); scale bar in (A4) is 10 µm; scale bar in (B) is 50 µm for (B, C); scale bar in (D) is 50 µm; scale bar in (E) is 100 µm.

relative thickness of the ON and OFF sublayers differs between species. These two cholinergic amacrine cell populations were also present in the fat dormouse (Fig. 5A). Their ChAT bands stratified at the S1/S2 boundary and in S3, respectively, locating the ON/OFF boundary of the IPL approximately to S2/S3.

Mammalian retinal bipolar cells show two basic divisions. One is a division into ca. 10 cone bipolar cell types that exclusively or predominantly contact cones, and one type of rod bipolar cell that predominantly contacts rods; the other division is that of the cone bipolar cells into functional ON cone bipolars and OFF cone bipolars, whereas the rod bipolar cell is ON (reviews: Wässle 2004, Euler et al. 2014). The axon terminals of all bipolar cells follow the ON/OFF stratification of the IPL. In the fat dormouse, we only assessed the rod bipolar cells (Fig. 5A). They formed a dense population with somata at the outer border of the INL, dendritic arbors in the OPL to contact the rods, and axon terminals at the inner edge of the IPL near the GCL, occupying S4 and S5. These are the typical rod bipolar cell properties also seen in nocturnal mammals like mouse and rat (see Discussion). The location of the axon terminals below the inner ChAT band clearly identifies the *G. glis* rod bipolars as ON cells as in all mammals.

Horizontal cells were labeled by parvalbumin and calbindin 28k antisera (Fig. 5B, C). Their somata were larger than those of bipolar cells and were located at the outer edge of the INL, their processes formed a dense plexus in the OPL. A flat-mounted calbindin-labeled retina showed the mosaic of the horizontal cell somata, which was rather regular without soma pairs (Fig. 5E). This may indicate a single type of horizontal cell because a mixed population of two types, as present in many mammals, would show a more irregular mosaic with many soma pairs (see Discussion). Neurofilament NF200 labeling also showed the plexus of presumed horizontal cell processes in the OPL, but no horizontal cell somata (Fig. 5D). Various *G. glis* amacrine cell types were parvalbumin-positive, calbindin-positive, or NF200-positive (Fig. 5B–D). Because

in the vertical sections their morphology was only partially revealed – the somata at the inner edge of the INL and the initial parts of the dendritic trees in the IPL – we cannot comment on their precise identity. The optic nerve fibre layer showed very intense NF200 labeling, as ganglion cell axons contain many neurofibrils; some larger ganglion cell somata also were NF200 labeled (Fig. 5D).

Retinal ganglion cells and visual acuity

The densities of presumed retinal ganglion cells (RGCs) and of all neurons (RGCs and displaced amacrine cells) in the *Glis glis* ganglion cell layer (GCL) were determined with an antibody to NeuN and with the general neuronal marker NeuroTrace, respectively (Fig. 6). Labeling for NeuN (identified as the protein Fox-3) is rather specific for RGCs (see discussion). In both *G. glis* and *Graphiurus*, the ubiquitous labeling of the neuronal nuclei of all retinal layers by NeuroTrace is obvious in Fig. 1. The NeuN label was restricted to the GCL, where it labeled a subpopulation of NeuroTrace-positive cells, with more intense labeling of the cytoplasm than the nucleus. The morphology of the NeuN-positive somata conforms to that of RGCs (Figs. 1, 6).

The $NeuN^-$ and NeuroTrace-positive cell densities in the GCL were counted in representative fields of one *G. glis* temporal half-retina, where the RGC density is expected to have its maximum in the region of highest cone density, the area centralis. Further counts were made in a *G. glis* nasal retinal piece to assess cell densities in mid-peripheral and peripheral retina, but no full topographic analysis was attempted.

The highest GCL neuron densities we found in temporal retina were ca. 4,000/mm² $NeuN^+$-positive presumed RGCs plus ca. 950/mm² NeuroTrace-positive but NeuN-negative neurons,

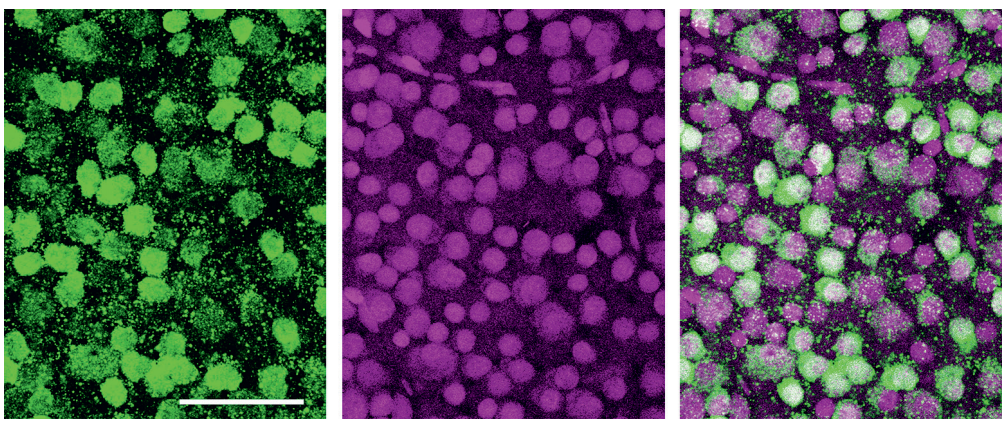

Fig. 6. *Glis glis* retinal ganglion cell layer. Left: NeuN label of presumed ganglion cells; middle: NeuroTrace label of all neurons of the GCL; right: merge of the images, colocalisation of both labels appears white. Field from central retina with a density of ca. 3,700 $NeuN^+$ somata/mm² and ca. 4,700 $NeuroTrace^+$ somata/mm². NeuN label intensity varies greatly across somata of different sizes, both the nuclei and the cytoplasm are labeled. The extracellular green punctate background label probably is a technical artefact. NeuroTrace label intensity is less variable, the nuclei are labeled more intensely than the cytoplasm. Scale bar is 50 µm.

Table 2. *Glis glis* main retinal features in comparison to other nocturnal rodents

	*Glis glis**	*Rattus norvegicus*	*Mus musculus*
rod density (1/mm²)	600,000–780,000	~374,000[1]	~437,000[2]
rod spectral tuning	?	498 nm[3]	498 nm[3]
peak cone density (1/mm²)	3,300	7000[4]	15,700[2]
mean cone %age of photoreceptors	~0.25–0.5%	0.85%[5]	~3%[2]
L cones present / tuning	yes / ?	yes / 509 nm[4]	yes / ~510 nm[6]
S cones present / tuning	no / UV (?)	yes / UV (359 nm)[4]	yes / UV (359 nm)[6]
RGC peak density (1/mm²)	~4,000	3,500[7]	5,850[8]
visual acuity	~1.8 cyc/deg (33') estimate	~1.0 cyc/deg (60') behaviour[9]	~0.5 cyc/deg (120') behaviour[9]

Data sources: *present study, [1]Mayhew & Astle (1997), [2]Jeon et al. (1998), [3]Bridges (1959), [4]Jacobs et al. (2001), [5]Szél & Röhlich (1992), [6]Jacobs et al. (2004), [7]Salinas-Navarro et al. (2009a), [8]Salinas-Navarro et al. (2009b), [9]Prusky et al. (2000).

which presumably are displaced amacrine cells, i.e., a maximal GCL neuron density of ca. 4,950/mm². It has to be noted, that we may not have recorded the highest neuron density present in the temporal retina. Density minima in peripheral retina were ca. 1,300/mm² $NeuN^+$ cells and 1,000/mm² $NeuroTrace^+/NeuN^-$ cells in dorsal periphery, ca. 1,100/mm² $NeuN^+$ cells and 600/mm² $NeuroTrace^+/NeuN^-$ cells in ventral periphery, and ca. 850/mm² $NeuN^+$ cells and 1,000/mm² $NeuroTrace^+/NeuN^-$ cells in nasal periphery. Among the total of NeuroTrace-positive GCL neurons the proportion of presumed displaced amacrine cells (NeuN-negative) was around 20% in central retina, 20–40% in mid-peripheral retina, and 40–60% in peripheral retina.

An estimate of the upper limit of the visual acuity of the fat dormouse was obtained from the maximal density of 4000 presumed RGCs/mm² and the axial length of 6.3 mm of the eye for which the RGC densities were obtained. With the equations given in the Methods section, the posterior nodal distance of this eye was 3.28 mm and the retinal magnification factor was 0.057 mm/deg. The visual acuity was 31.62 cycles per mm on the retina, which converts to 1.80 cycles per degree of visual angle, or 33 minutes of arc. The caveats associated with this estimate are addressed in the discussion.

DISCUSSION

The present study provides the first description of retinal structure in the rodent family Gliridae, with a more detailed analysis for the European fat dormouse *Glis glis* than for the African dormouse *Graphiurus* sp. Our main findings are summarised in Table 2, comparing them to the corresponding retinal features in the rat and mouse, which are intensely studied nocturnal rodents.

R o d s

Mammalian retinae show marked evolutionary adaptations to the diel activity pattern of the species, e.g., nocturnal or diurnal. This is particularly obvious in the photoreceptor complement. Nocturnal mammals possess higher densities of the more sensitive rod photoreceptors that are used for low-light vision, and lower proportions of the cone photoreceptors used for daylight and colour vision (for overviews see, e.g., Ahnelt & Kolb 2000, Peichl 2005). However, the

very high rod densities of up to 780,000/mm² found in *G. glis* are unusual even for nocturnal mammals. For example, the Norway rat has about 374,000 rods/mm² (Mayhew & Astle 1997), and the house mouse about 437,000 rods/mm² (Jeon et al. 1998). Among the few known species with comparably high rod densities in the range of 700,000–800,000/mm² are the African pouched rats (*Cricetomys*) and some fruit bats (Peichl & Moutairou 1998, Müller et al. 2007). The estimated *Graphiurus* rod density of about 395,000–490,000/mm² is more similar to that of rat and mouse. It is unclear what adaptive advantage is associated with the particularly high rod density in *Glis glis*, considering that other nocturnal rodents obviously manage with lower rod densities. Interestingly, the subterranean bathyergid mole-rats have photoreceptor densities of only 100,000–150,000/mm², of which ca. 10% are cones (Peichl et al. 2004). Perhaps in their lightless tunnel habitats, there was no adaptive pressure to invest in a very light-sensitive photoreceptor outfit, so they retained an all-purpose photoreceptor set for instances when they come to the surface or encounter a tunnel breach.

Our data on the inverted rod nuclear architecture in *G. glis* and *Graphiurus* show that it conforms to that found in all nocturnal mammals studied to date (Solovei et al. 2009). As detailed by Irina Solovei and colleagues (Solovei et al. 2009, Feodorova et al. 2020), the central position of the inactive heterochromatin and peripheral position of the active euchromatin are assumed to be strongly disadvantageous for nuclear functions, but they have a positive effect on retinal optics. The densely packed heterochromatin core is highly refractive and shows the physical properties of a light-focusing lens. Hence, the rod nuclei in the ONL form columns of microlenses that act as 'light guides'. This strongly reduces light scattering in the ONL, which is particularly important for nocturnal mammals with their thick ONL and the need to capture as many of the precious few photons available at night. Obviously, inverted rod nuclei are an evolutionary adaptation to improve nocturnal vision.

Cones

Our findings show that *Glis glis* and *Graphiurus* are L cone monochromats and hence most likely colour-blind. Very limited colour discrimination may be possible at intermediate, 'mesopic' light levels by the interaction of the L cones and rods (review: Jacobs 2013). However, the L cone tuning is probably at ca. 510 nm, as is common in species with UV-tuned S cones, and the rod tuning is probably at ca. 500 nm as in most mammals, so the tuning difference available for colour discrimination probably is minimal.

As reviewed by Jacobs (2013), there is a growing number of mostly nocturnal mammals that are shown to have lost their S cone function. The list currently comprises 75 species from five different orders. In some instances, the loss is common to the entire clade (Cetacea, Pinnipedia), in others it is limited to a genus or possibly a single species. The two dormouse species studied here can be added to this list. The S cone absence in both *Glis glis* and *Graphiurus* may indicate that the loss has occurred across the family Gliridae. This would need confirmation by studying further species of the family. The substantial number of nocturnal mammals that have lost their S cones indicates that colour vision is not a crucial requirement for survival when being active at low light levels. On the other hand, the presence of L cones and S cones and hence the potential for dichromatic colour vision in most nocturnal mammals indicates that an S cone loss is not necessarily an adaptive advantage in a nocturnal lifestyle. At present, there is no single convincing explanation for the S cone loss, and various scenarios are considered by Jacobs (2013).

The SWS1 tuning is determined by the amino acids present at a few critical positions in exon 1, the most important being site 86 with Phe present in UVS pigments, and commonly either Tyr or Leu in VS pigments (Cowing et al. 2002, Fasick et al. 2002). We show that exon 1 of the *G. glis* SWS1 opsin has the same tuning-relevant amino acids as the UV-tuned SWS1 of the mouse and rat (Table 1). Hence, the *G. glis* SWS1 opsin, if expressed, would have resulted in a UV-tuned visual pigment. UV tuning is the ancestral state of the SWS1 opsin. In many mammals it has shifted to a violet or blue tuning during evolution, but in some nocturnal mammals, including a number of nocturnal rodents, the shift has not occurred (reviews: Hunt et al. 2007, Jacobs 2009, Hunt & Peichl 2014). One view is that nocturnal mammals are habitually exposed to low light levels and hence also low UV levels, so no protective measures like UV-blocking lenses needed to be evolved to prevent damaging UV intensities from reaching the retina (review: Douglas & Jeffery 2014). Consequently, there was no pressure to shift the SWS1 pigment to the longer wavelengths that reach the retina through a UV-blocking lens. On the other hand, a number of mammals with violet-to-blue-sensitive SWS1 pigments also have lenses that transmit significant amounts of UV (Douglas & Jeffery 2014). The authors report that UV-blocking lenses are primarily found in species with high cone densities and high visual acuity. On both accounts, an exposure to only low UV intensities, and a very low cone density and poor visual acuity, the fat dormouse belongs to the species in which UV tuning of the SWS1 opsin would be expected.

Interneurons

The few interneurons that we have stained in the *Glis glis* retina are very similar to those found in the mouse retina (see, e.g., Haverkamp & Wässle 2000). Nocturnal (scotopic) vision depends on the retinal signaling pathways of the rods, in which the single type of rod bipolar cell is a key component (review: Euler et al. 2014). Rod bipolar cells can be consistently labeled by antibodies to PKCα, which facilitates their comparative study (Greferath et al. 1990). The rod bipolar cells of *G. glis* appear morphologically similar to those of mouse and rat (Wässle et al. 1991, Haverkamp & Wässle 2000; also see images at http://retinalmicroscopy.com/bipolar-cells, accessed on 22 August 2022). As expected for a nocturnal mammal with a high rod density, the *G. glis* rod bipolars also have a high population density, and their axon terminal systems occupy a relatively large proportion of the IPL thickness, namely the innermost two of the five IPL substrata (Fig. 5A4). In the nocturnal South American opossum *Monodelphis domestica*, the numerous rod bipolars even occupy the three strata S3–S5 (Lutz et al. 2018). In diurnal primates and the diurnal *Octodon degus*, the rod bipolar cell density is lower, and their axon terminal proportion of the IPL is less thick (http://retinalmicroscopy.com/bipolar-cells).

The amacrine cells are the morphologically and functionally most diverse retinal cell group, and only a few of the types have been studied in detail (reviews: Vaney 1990, Masland 2012). The cholinergic amacrine cells, also termed 'starburst amacrine cells' because of their distinctive radially symmetric dendritic trees, are one of the well-studied types. They have been found across mammals and play a crucial role in shaping the directional selective response of direction-selective ganglion cells (review: Vaney et al. 2012). They come as OFF and ON subpopulations with their somata in the INL and GCL, respectively, and their dendritic trees stratifying in the OFF and ON sublayer of the IPL, respectively. This stratification pattern is a useful indicator of the functional subdivision of the IPL. We could show that the fat dormouse also has these cholinergic amacrine cells. This suggests that *G. glis* has direction selective ganglion cells.

The blueprint of the mammalian retina contains two horizontal cell types, the axonless A-type that contacts only cones, and the axon-bearing B-type that contacts cones with its dendrites and rods with its axons (review: Peichl 2010). However, the murid rodents mouse, rat and gerbil only have the B-type (Peichl & González-Soriano 1994). Our data do not show whether *G. glis* has two horizontal cell types or one, but the regularity of the horizontal cell soma mosaic indicates that it may only have one type (Fig. 5E). Retinal cell types typically form regular mosaics, and the superposition of the regular mosaics of two horizontal cell populations with different densities would result in a less regular mosaic with many soma pairs (Wässle et al. 1978, Peichl & González-Soriano 1994). A more detailed morphological analysis is necessary to determine whether the fat dormouse has one or two horizontal cell types.

Ganglion cells and visual acuity

The retinal ganglion cells (RGCs) are the output stages of retinal processing. Their peak densities determine the maximal visual acuity, representing the sampling density (pixel density) of image processing. With the neuronal markers NeuroTrace and NeuN we determined the densities of all neurons (RGCs and displaced amacrine cells) and of presumed RGCs in the ganglion cell layer of *Glis glis* in one temporal half-retina, where the RGC density is expected to have its maximum in the region of highest cone density, the area centralis. In the retina, labeling for NeuN is rather specific for RGCs (Buckingham et al. 2008 and references therein). The *G. glis* proportion of presumed displaced amacrine cells (NeuroTrace$^+$ and NeuN$^-$) in the GCL is ca. 20% in central retina, 20–40% in mid-peripheral retina, and 40–60% in peripheral retina. This proportion is roughly comparable to those in rat and mouse (rat: ca. 50% displaced amacrines, Perry 1981; mouse: ca. 60% displaced amacrines, Jeon et al. 1998).

The broad range of RGC soma sizes seen in Fig. 6 indicates the presence of several morphological types with different dendritic field morphologies and hence receptive field sizes and response properties. These could not be assessed in the present study. For example, mouse RGCs have been classified into more than 40 types by morphological, physiological, and molecular features (see, e.g., Goetz et al. 2022).

With the highest RGC density and the axial length of the studied *G. glis* eye, its maximal visual acuity is estimated as ca. 1.8 cycles/degree or 33 min of arc. This acuity would be nearly twice as good as that of the rat (ca. 1 cyc/deg; Prusky et al. 2000) and nearly four times as good as that of the mouse (ca. 0.5 cyc/deg; Prusky et al. 2000). However, the rat and mouse acuities were determined behaviourally, and there are two caveats concerning our anatomical acuity estimate. First, it is possible that some NeuroTrace-positive nuclei without NeuN label also are RGCs, which would increase the RGC density and hence the visual acuity estimate. This is a realistic possibility, because some of the NeuN-negative somata are as large as medium- to large-sized NeuN-positive somata, whereas displaced amacrine cells in other species are known to have soma sizes at the lower end of the RGC spectrum. Second, not all RGC types contribute to visual acuity, only the types with the smallest receptive fields are involved in high acuity vision, which will make the real acuity smaller than our estimate. In the cat, for example, only the beta type RGCs with their small receptive fields set the limit of visual acuity, and they make up ca. 50% of the RGCs (review: Wässle & Boycott 1991). As we do not know the *G. glis* RGC types and their receptive field sizes, we cannot guess which proportion of the RGCs actually contributes to visual acuity. If, for the sake of argument, we speculate that only about 50% of the *G. glis* RGCs contribute to visual acuity, the acuity estimate goes down to 1.3 cyc/deg.

Acknowledgements

This article is dedicated to Professor Hynek Burda on the occasion of his 70th birthday.

We are grateful to Erwin Noll, Vladimir Lebedev and Svetlana Romanenko for their help with obtaining the eyes, to Gerlinde Heiss-Herzberger and Elke Laedtke for their skilled technical assistance, and to Jeremy Nathans and Robert S. Molday for providing opsin antibodies. This research was supported using resources of the VetCore Facility (Transcriptomics unit) of the University of Veterinary Medicine Vienna.

REFERENCES

Ahnelt P. K. & Kolb H., 2000: The mammalian photoreceptor mosaic: adaptive design. *Progress in Retinal and Eye Research*, **19**: 711–777.

Ahnelt P. K., Moutairou K., Glösmann M. & Kübber-Heiss A., 2003: Lack of S-opsin expression in the brush-tailed porcupine (*Atherurus africanus*) and other mammals. Is the evolutionary persistence of S-cones a paradox? Pp. 31–38. In: Mollon J. D., Pokorny J. & Knoblauch K. (eds.): *Normal and Defective Colour Vision*. Oxford University Press, Oxford, UK, 460 pp.

Bridges C. D., 1959: Visual pigments of some common laboratory mammals. *Nature*, **184**(Supplement 22): 1727–1728.

Buckingham B. P., Inman D. M., Lambert W., Oglesby E., Calkins D. J., Steele M. R., Vetter M. L., Nicholas Marsh-Armstrong N. & Horner P. J., 2008: Progressive ganglion cell degeneration precedes neuronal loss in a mouse model of glaucoma. *Journal of Neuroscience*, **28**: 2735–2744.

Büchner S., Trout R. & Adamík P., 2018: Conflicts with *Glis glis* and *Eliomys quercinus* in households: a practical guideline for sufferers (Rodentia: Gliridae). *Lynx*, *n.s.*, **49**: 19–26.

Cowing J. A., Poopalasundaram S., Wilkie S. E., Robinson P. R., Bowmaker J. K. & Hunt D. M., 2002: The molecular mechanism for the spectral shifts between vertebrate ultraviolet- and violet-sensitive cone visual pigments. *Biochemical Journal*, **367**: 129–135.

Damsgaard C. & Country M. W., 2022: The opto-respiratory compromise: balancing oxygen supply and light transmittance in the retina. *Physiology*, **37**: 101–113.

Douglas R. H. & Jeffery G., 2014: The spectral transmission of ocular media suggests ultraviolet sensitivity is widespread among mammals. *Proceedings of the Royal Society B*, **281**(20132995): 1–9.

Euler T., Haverkamp S., Schubert T. & Baden T., 2014: Retinal bipolar cells: elementary building blocks of vision. *Nature Reviews Neuroscience*, **15**: 507–519.

Fasick J. I., Applebury M. L. & Oprian D. D., 2002: Spectral tuning in the mammalian short-wavelength sensitive cone pigments. *Biochemistry*, **41**: 6860–6865.

Feodorova Y., Falk M., Mirny L. A. & Solovei I., 2020: Viewing nuclear architecture through the eyes of nocturnal mammals. *Trends in Cell Biology*, **30**: 276–289.

Goetz J., Jessen Z. F., Jacobi A., Mani A., Cooler S., Greer D., Kadri S., Segal J., Shekhar K., Sanes J. R. & Schwartz G. W., 2022: Unified classification of mouse retinal ganglion cells using function, morphology, and gene expression. *Cell Reports*, **40**(111040): 1–17+1–5.

Greferath U., Grünert U. & Wässle H., 1990: Rod bipolar cells in the mammalian retina show protein kinase C-like immunoreactivity. *Journal of Comparative Neurology*, **301**: 433–442.

Haverkamp S. & Wässle H., 2000: Immunocytochemical analysis of the mouse retina. *Journal of Comparative Neurology*, **424**: 1–23.

Hemmi J. M. & Grünert U., 1999: Distribution of photoreceptor types in the retina of a marsupial, the tammar wallaby (*Macropus eugenii*). *Visual Neuroscience*, **16**: 291–302.

Hicks D. & Molday R. S., 1986: Differential immunogold-dextran labeling of bovine and frog rod and cone cells using monoclonal antibodies against bovine rhodopsin. *Experimental Eye Research*, **42**: 55–71.

Hunt D. M. & Peichl L., 2014: S cones: Evolution, retinal distribution, development, and spectral sensitivity. *Visual Neuroscience*, **31**: 115–138.

Hunt D. M., Carvalho L. S., Cowing J. A., Parry J. W., Wilkie S. E., Davies W. L. & Bowmaker J. K., 2007: Spectral tuning of shortwave-sensitive visual pigments in vertebrates. *Photochemistry and Photobiology*, **83**: 303–310.
Jacobs G. H., 2009: Evolution of colour vision in mammals. *Philosophical Transactions of the Royal Society B*, **364**: 2957–2967.
Jacobs G. H., 2013: Losses of functional opsin genes, short-wavelength cone photopigments, and color vision – A significant trend in the evolution of mammalian vision. *Visual Neuroscience*, **30**: 39–53.
Jacobs G. H., Neitz J. & Crognale M., 1985: Spectral sensitivity of ground squirrel cones measured with ERG flicker photometry. *Journal of Comparative Physiology A*, **156**: 503–509.
Jacobs G. H., Neitz J. & Deegan J. F., 1991: Retinal receptors in rodents maximally sensitive to ultraviolet light. *Nature*, **353**: 655–656.
Jacobs G. H., Fenwick J. A. & Williams G. A., 2001: Cone-based vision of rats for ultraviolet and visible lights. *Journal of Experimental Biology*, **204**: 2439–2446.
Jacobs G. H., Williams G. A. & Fenwick J. A., 2004: Influence of cone pigment coexpression on spectral sensitivity and color vision in the mouse. *Vision Research*, **44**: 1615–1622.
Jeon C. J., Strettoi E. & Masland R. H., 1998: The major cell populations of the mouse retina. *Journal of Neuroscience*, **18**: 8936–8946.
Kirk E. C., 2006: Eye morphology in cathemeral lemurids and other mammals. *Folia Primatologica*, **77**: 27–49.
Kolmer W., 1936: Kapitel X. Die Netzhaut (Retina). Pp. 295–468. In: Kolmer W. & Lauber H. (eds.): *Handbuch der mikroskopischen Anatomie des Menschen*. *Dritter Band*: *Haut und Sinnesorgane*. *Zweiter Teil*: *Auge*. Verlag Julius Springer, Berlin, 782 pp.
Kryštufek B., 2010: *Glis glis* (Rodentia: Gliridae). *Mammalian Species*, **42**(865): 195–206.
Land M. F. & Nilsson D.-E., 2002: *Animal Eyes*. Oxford University Press, Oxford, 221 pp.
Lutz N. D., Lemes E., Krubitzer L., Collin S. P., Haverkamp S. & Peichl L., 2018: The rod signaling pathway in marsupial retinae. *Public Library of Science One*, **13**(8; e0202089): 1–19.
Masland R. H., 2012: The tasks of amacrine cells. *Visual Neuroscience*, **29**: 3–9.
Mayhew T. M. & Astle D., 1997: Photoreceptor number and outer segment disk membrane surface area in the retina of the rat: stereological data for whole organ and average photoreceptor cell. *Journal of Neurocytology*, **26**: 53–61.
Müller B., Goodman S. M. & Peichl L., 2007: Cone photoreceptor diversity in the retinas of fruit bats (Megachiroptera). *Brain*, *Behavior and Evolution*, **70**: 90–104.
Müller B., Glösmann M., Peichl L., Knop G. C., Hagemann C. & Ammermüller J., 2009: Bat eyes have ultraviolet-sensitive cone photoreceptors. *Public Library of Science One*, **4**(7; e6390): 1–7.
Oprian D. D., Asenjo A. B., Lee N. & Pelletier S. L., 1991: Design, chemical synthesis, and expression of genes for the three human color vision pigments. *Biochemistry*, **30**: 11367–11372.
Parry J. W. L. & Bowmaker J. K., 2002: Visual pigment coexpression in guinea pig cones: A microspectrophotometric study. *Investigative Ophthalmology & Visual Science*, **43**: 1662–1665.
Peichl L., 2005: Diversity of mammalian photoreceptor properties: Adaptations to habitat and lifestyle? *Anatomical Record*, *Part A*, *Discoveries in Molecular*, *Cellular*, *and Evolutionary Biology*, **287A**: 1001–1012.
Peichl L., 2010: Morphology of interneurons: Horizontal cells. Pp. 74–82. In: Dartt D. A. (ed.): *Encyclopedia of the Eye*. *Volume 3*. Academic Press, Oxford, 555 pp.
Peichl L. & González-Soriano J., 1994: Morphological types of horizontal cell in rodent retinae: A comparison of rat, mouse, gerbil and guinea pig. *Visual Neuroscience*, **11**: 501–517.
Peichl L. & Moutairou K., 1998: Absence of short-wavelength sensitive cones in the retinae of seals (Carnivora) and African giant rats (Rodentia). *European Journal of Neuroscience*, **10**: 2586–2594.
Peichl L., Němec P. & Burda H., 2004: Unusual cone and rod properties in subterranean African mole-rats (Rodentia, Bathyergidae). *European Journal of Neuroscience*, **19**: 1545–1558.
Perry V. H., 1981: Evidence for an amacrine cell system in the ganglion cell layer of the rat retina. *Neuroscience*, **6**: 931–944.

Pettigrew J. D., Dreher B., Hopkins C. S., McCall M. J. & Brown M., 1988: Peak density and distribution of ganglion cells in the retinae of microchiropteran bats: Implications for visual acuity. *Brain, Behavior and Evolution*, **32**: 39–56.

Prusky G. T., West P. W. R. & Douglas R. M., 2000: Behavioral assessment of visual acuity in mice and rats. *Vision Research*, **40**: 2201–2209.

Salinas-Navarro M., Mayor-Torroglosa S., Jiménez-López M., Avilés-Trigueros M., Holmes T. M., Lund R. D., Villegas-Pérez M. P. & Vidal-Sanz M., 2009a: A computerized analysis of the entire retinal ganglion cell population and its spatial distribution in adult rats. *Vision Research*, **49**: 115–126.

Salinas-Navarro M., Jiménez-López M., Valiente-Soriano F. J., Alarcón-Martínez L., Avilés-Trigueros M., Mayor S., Holmes T., Lund R. D., Villegas-Pérez M. P. & Vidal-Sanz M., 2009b: Retinal ganglion cell population in adult albino and pigmented mice: A computerized analysis of the entire population and its spatial distribution. *Vision Research*, **49**: 637–647.

Schmitz L. & Motani R., 2010: Morphological differences between the eyeballs of nocturnal and diurnal amniotes revisited from optical perspectives of visual environments. *Vision Research*, **50**: 936–946.

Solovei I., Kreysing M., Lanctôt C., Kösem S., Peichl L., Cremer T., Guck J. & Joffe B., 2009: Nuclear architecture of rod photoreceptor cells adapts to vision in mammalian evolution. *Cell*, **137**: 356–368.

Szél Á. & Röhlich P., 1992: Two cone types of rat retina detected by anti-visual pigment antibodies. *Experimental Eye Research*, **55**: 47–52.

Vaney D. I., 1990: The mosaic of amacrine cells in the mammalian retina. *Progress in Retinal Research*, **9**: 49–100.

Vaney D. I., Sivyer B. & Taylor W. R., 2012: Direction selectivity in the retina: symmetry and asymmetry in structure and function. *Nature Reviews Neuroscience*, **13**: 194–208.

Wang Y., Macke J. P., Merbs S. L., Zack D. J., Klaunberg B., Bennett J., Gearhart J. & Nathans J., 1992: A locus control region adjacent to the human red and green visual pigment genes. *Neuron*, **9**: 429–440.

Wässle H., 2004: Parallel processing in the mammalian retina. *Nature Reviews Neuroscience*, **5**: 747–757.

Wässle H. & Boycott B. B., 1991: Functional architecture of the mammalian retina. *Physiological Reviews*, **71**: 447–480.

Wässle H., Peichl L. & Boycott B. B., 1978: Topography of horizontal cells in the retina of the domestic cat. *Proceedings of the Royal Society of London B*, **203**: 269–291.

Wässle H., Yamashita M., Greferath U., Grünert U. & Müller F., 1991: The rod bipolar cell of the mammalian retina. *Visual Neuroscience*, **7**: 99–112.